EXPERIMENTAL MEASUREMENT OF DIAPHRAGM DEFORMATION AND BURSTING IN A TWO-STAGE LIGHT GAS GUN

57th Meeting of the Aeroballistic Range Association, 2006-09-18 – 2006-09-22, Venice, Italy

Robin Putzar[1], Guy Spencer[1,2], Frank Schaefer[1]

[1]Fraunhofer Institute for High-Speed Dynamics, Ernst-Mach-Institut, Eckerstr. 4, 79104 Freiburg, Germany
[2]Air Force Office of Scientific Research, United States Air Force, 875 N. Randolph St. Suite 325, Room 3112, Arlington VA 22203, USA
robin.putzar@emi.fhg.de; guy.spencer@kirtland.af.mil; frank.schaefer@emi.fhg.de

ABSTRACT

The burst process of steel diaphragms that are used in two-stage light gas guns to seal the pump tube from launch tube was investigated. Four experiments were performed, in which diaphragm surface velocity and the pressure acting upon the diaphragm were measured during standard gun cycles without projectile or sabot. The measurements indicate that shocks are travelling inside the pump tube, tearing the diaphragm open when the pressure is high enough. The diaphragms investigated burst at a pressure between 30 and 37 MPa.

The pressure signals obtained are superposed by considerable noise. The two major contributors to this noise are identified as (1) natural oscillation of the pressure sensor and (2) standing sound waves in the pressure sensor drill hole, both excited by the shocks travelling along the pump tube.

INTRODUCTION

In the area of hypervelocity impact research, accelerators are needed which can reproducibly accelerate almost arbitrarily shaped objects to high velocities. Currently two-stage light gas guns are the most capable accelerators for projectiles with masses ranging from hundreds of micrograms to kilograms. The Fraunhofer Institute for High-Speed Dynamics, Ernst-Mach-Institut (EMI) operates several two-stage light gas guns [1, 2], performing basic hypervelocity research as well as project research [3-11].

Deeper knowledge of the acceleration process is needed to allow further optimisation of the performance of this type of gun. In an effort to understand the initial part of the acceleration process, the deformation and bursting of the steel diaphragm separating the pump tube from the launch tube was investigated. The investigations were performed during standard gun firings without sabot. The measurements are therefore regarded as being more realistic than those obtained from e. g. quasi-static inflation testing.

EXPERIMENTAL SET-UP, MEASUREMENTS AND SIGNAL CONDITIONING

The experiments were performed at the Space Light Gas Gun at Fraunhofer EMI. The gun is based on the two-stage light gas gun principle [1, 9], see Figure 1. This gun is capable of launching millimetre-sized projectiles with masses between 1 mg and 500 mg to velocities from 2 km/s to above 9 km/s.

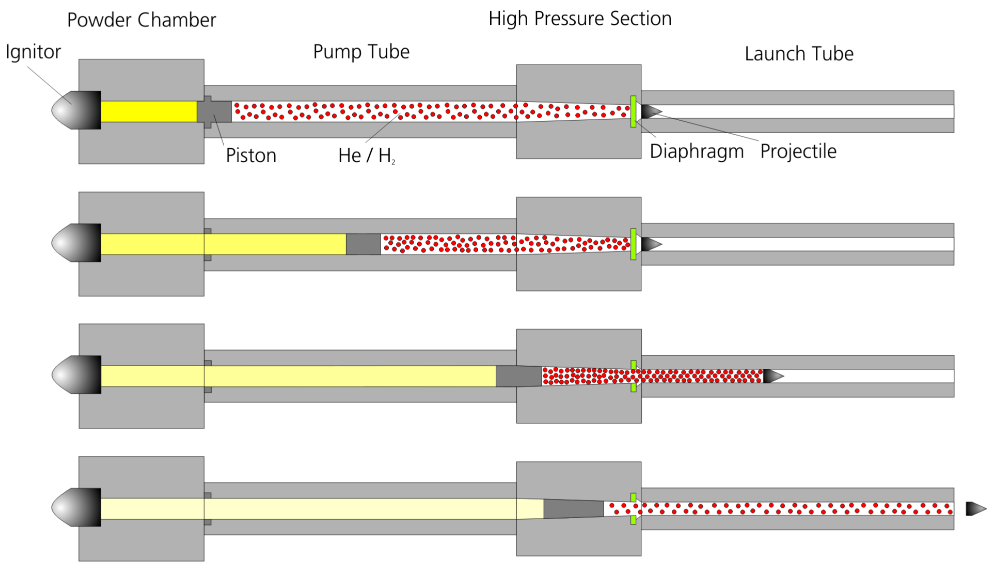

Figure 1: Two-stage light gas gun cycle.

For the diaphragm burst experiments, the gun was prepared as for a normal shot. As the only modification, neither projectile nor sabot was used, resulting in an undisturbed view through the launch tube from muzzle to diaphragm. The driving gas was Hydrogen.

The type of steel diaphragm investigated is shown in Figure 2 and Figure 3. The thickness of the diaphragms amounts to 1.50 mm. The cross-forming grooves are 15 mm long and 1.6 mm wide. The residual material thickness amounts to 0.5 mm in the centre. The diaphragm outer diameter is 45 mm. To improve reflection of the laser beam, a reflective foil is attached to the rear side of the diaphragm.

Diaphragm oscillation was measured using a laser vibrometer (LV) from Polytec (sensor head OFV-505, control unit OFV-5000 with velocity decoder VD-02 and displacement decoder DD-100). This device is capable of measuring vibration speeds up to 10 m/s with frequencies up to 1.5 MHz and vibration displacements up to 163 mm with frequencies up to 250 kHz. The LV beam was oriented via a mirror in the blast chamber towards the diaphragm. The set-up is shown in Figure 4. For each experiment, a new mirror was required.

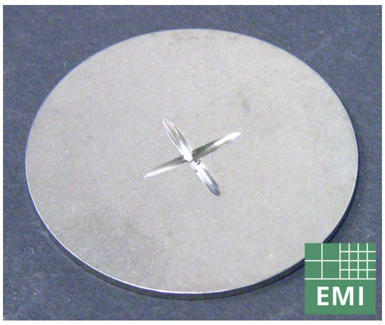

Figure 2: Diaphragm before experiment, front side.

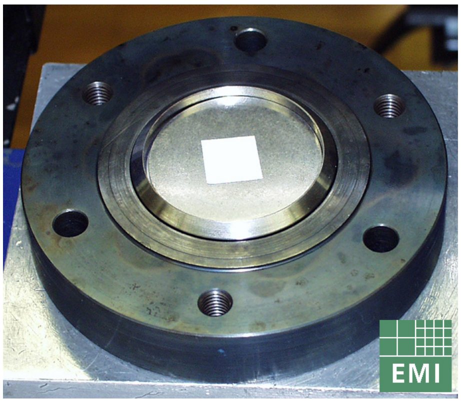

Figure 3: Diaphragm in support with reflecting foil attached to rear side.

In all experiments, the pressure in the high pressure section (HPS) was measured (102 mm in front of the diaphragm) by a Kistler quartz high-pressure-sensor (type 6213B) connected to a Kistler charge amplifier (type 5011). A 6 mm long drill hole connected the sensor active area to the HPS gas volume, see Figure 5.

The LV and charge amplifier outputs were connected to an oscilloscope (Tektronix type TDS7254B). The time axes for all signals are consistent, but arbitrary (the oscilloscope was triggered when the signal of the HPS sensor exceeded 1 V). All sensor signals were filtered using a low pass at the cut-off frequency of the respective sensors: velocity at 1.5 MHz, displacement at 250 kHz and pressure at 200 kHz.

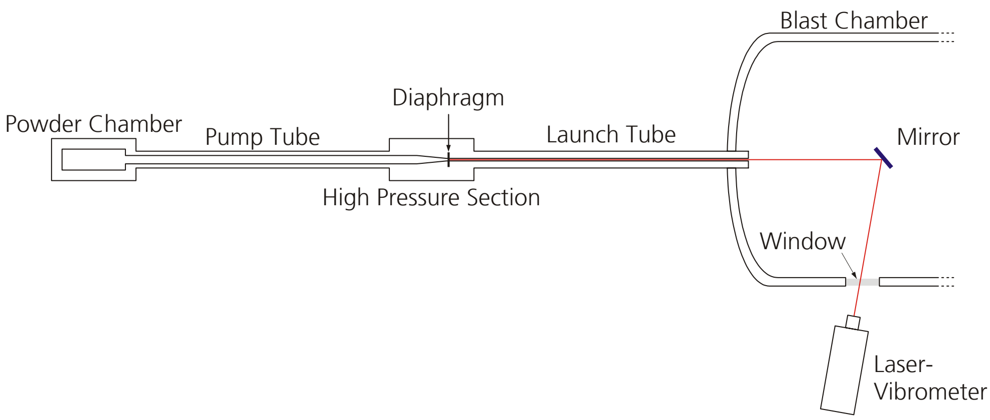

Figure 4: Schematic set-up (not to scale).

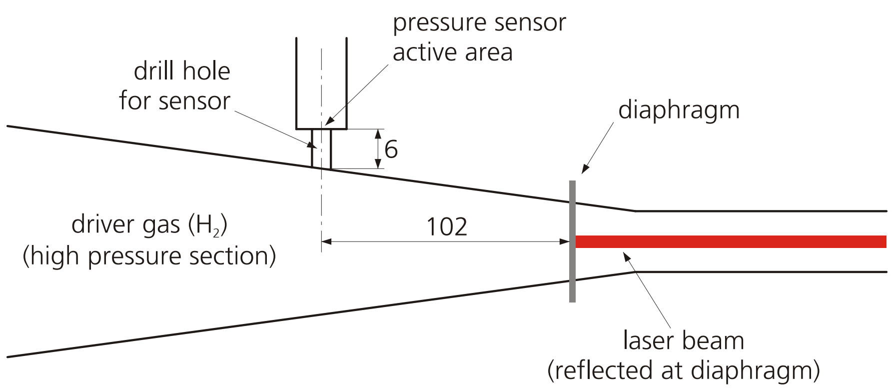

Figure 5: Set-up, close-up of high pressure section (not to scale, distances in mm).

EXPERIMENTAL RESULTS

Four experiments with different powder charge weight have been conducted. The initial pump tube pressure has been maintained at 0.6 MPa (6 bar). Table 1 summarises the main experimental parameters along with the maximum pressures recorded. Figure 6 shows the maximum recorded pressure versus powder load.

Table 1: Main experimental parameters and some measurement values.

Experiment	Powder Charge [g]	Pump Tube Initial Pressure [MPa]	max. Pressure in HPS [MPa]
4835	50	0.6	220
4838	50	0.6	240
4839	70	0.6	510
4840	75	0.6	520

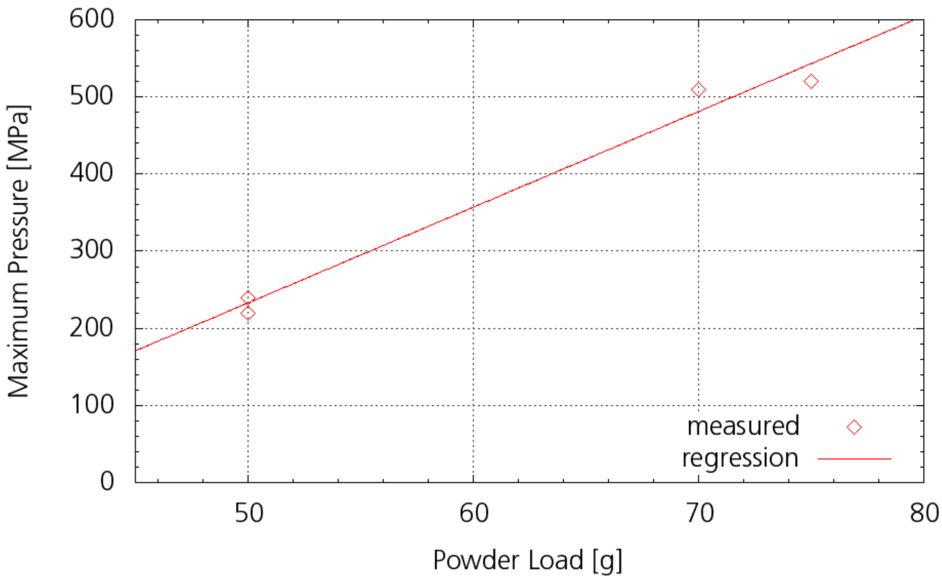

Figure 6: Maximum pressure in HPS as function of powder load.

The following two figures show the signals measured during experiment 4840 as an example. Figure 7 shows diaphragm surface velocity, diaphragm surface displacement (both measured in the centre of the diaphragm) and HPS pressure. Figure 8 is horizontally zoomed, showing diaphragm surface velocity and HPS pressure shortly before the diaphragm ruptures.

The signals show that the diaphragm was exposed to shocks generated inside the pump tube during compression of the light gas. The shock arrival times are marked by vertical lines. At –957 µs, the diaphragm was excited by a shock for the first time and started to oscillate (see the surface velocity plot of Figure 7). The measured oscillation frequency is 40 kHz, the maximum measured surface velocity is 1.1 m/s, and the maximum measured surface displacement is 10 µm. According to the displacement signal the diaphragm was deflected towards the LV, oscillating back into its original position.

At –355 µs, the diaphragm was excited by a second shock. The measured oscillation frequency is 30 kHz. The intensity of this shock caused the surface velocity to exceed the measurement range of the laser vibrometer (± 10 m/s). The maximum measured surface displacement was 60 µm, but since the maximum measurable velocity was exceeded, the real surface displacement might have been higher than that. Again, this shock deflected the diaphragm, which oscillated back close to its original position afterwards.

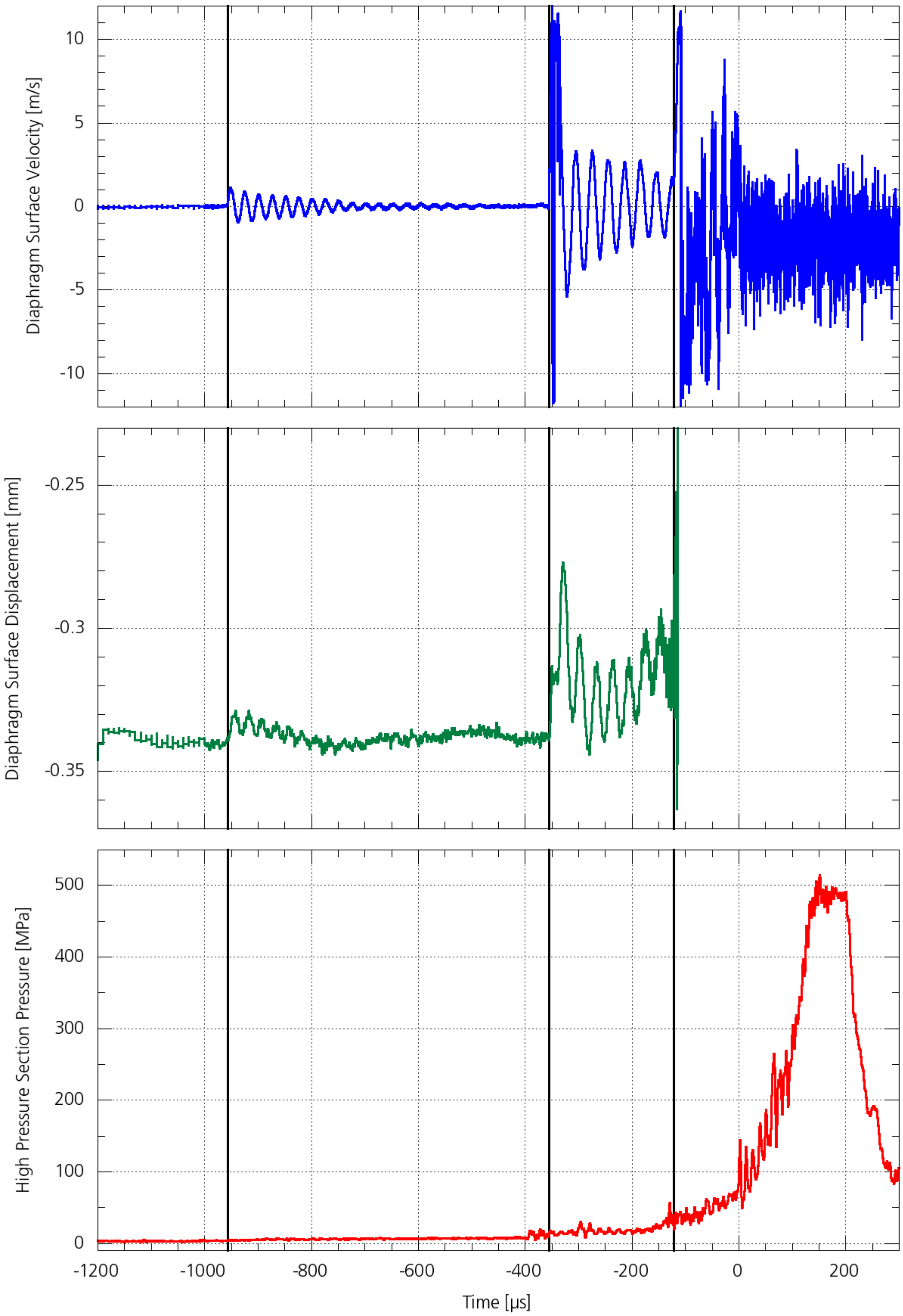

Figure 7: Velocity, displacement and pressure in HPS, experiment 4840.

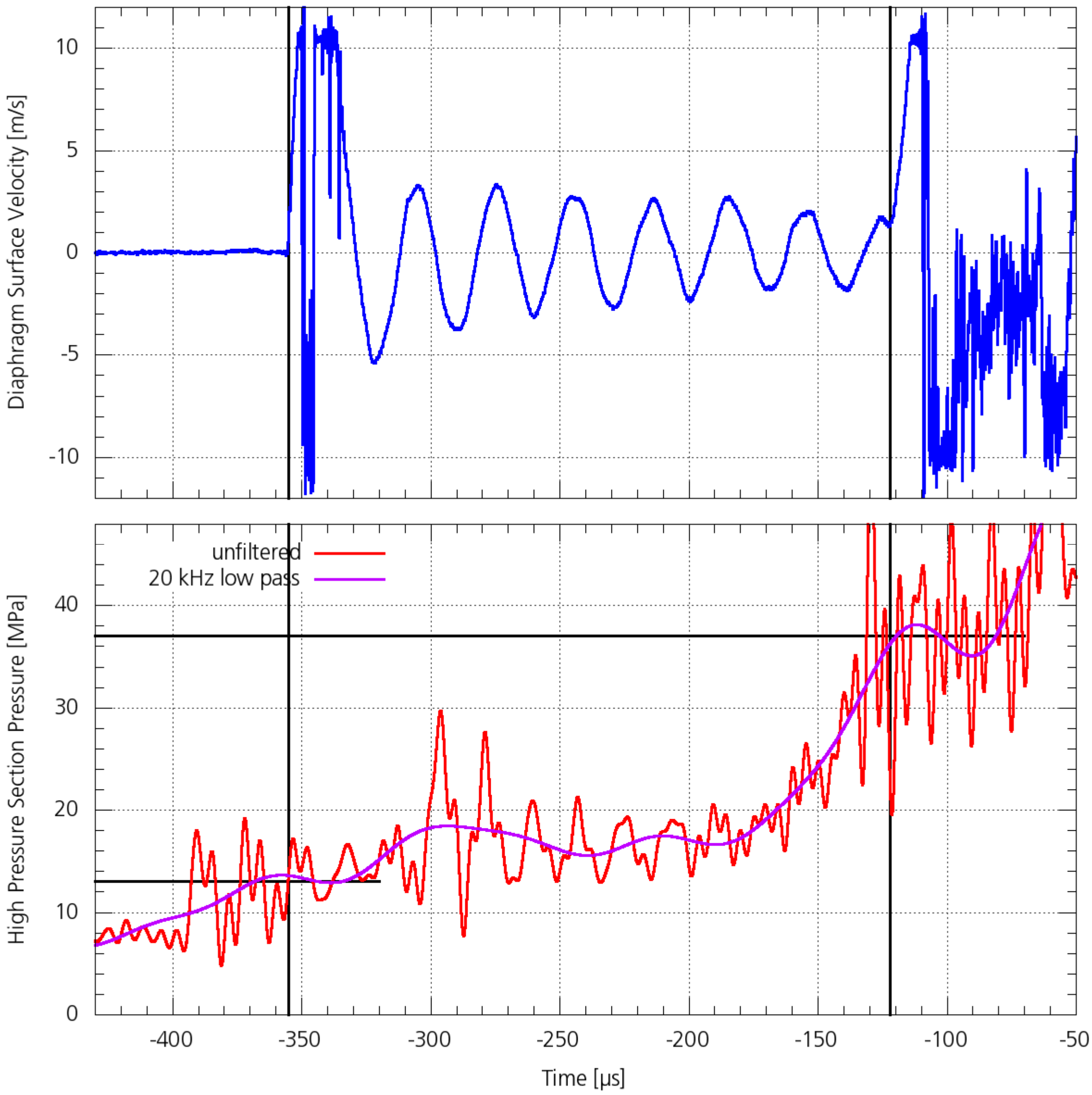

Figure 8: Velocity and pressure in HPS, shortly before rupture of the diaphragm, experiment 4840.

At –122 µs, a third shock arrived at the diaphragm. As no meaningful velocity or displacement was measured afterwards, it is assumed that this shock caused the diaphragm to rupture.

The pressure signal is superposed by considerable noise. The two major contributors to this noise are supposedly (1) the excitation of the pressure sensor's eigenfrequency by the shocks travelling along the pump tube, and (2) standing sound waves generated in the drill hole between pressure sensor and HPS, caused by the shocks as well. To reduce the effects of this noise, the pressure signal has been filtered by a 20 kHz low pass.

It should be noted that the HPS pressure reaches values similar to those obtained from experiments with similar loading conditions during earlier campaigns even in the absence of the sabot / projectile package.

EFFECTS OF SHOCKS ON DIAPHRAGM

To further analyse the measured signals, Figure 9 shows the HPS pressure shortly after shock arrival at the diaphragm, plotted versus shock arrival time. For an easier comparison between the experiments, the time axes of the individual experiments are shifted against each other. It should be noted that the data from experiments 4835 and 4838 (being conducted with the same experimental parameters) agree well; the shock arrival times differ only by approximately ten microseconds.

In all experiments except 4835, the LV beam was carefully adjusted to point to the centre of the diaphragm. In experiment 4835 (the first to be conducted), however, such careful adjustment was not made, and the beam was found to point near the rim of the diaphragm. For a centred LV beam, slight opening of the diaphragm suffices to interrupt the LV signal. In contrast, if the LV beam points to the rim, the LV signal can be received after a slight opening of the diaphragm.

It is assumed that this is the reason for five shocks being recorded in experiment 4835, in contrast to four shocks in experiment 4838. The diaphragm in experiment 4835 was presumably opened slightly by the fourth shock, but only the fifth shock opened it far enough for the LV beam to be interrupted. In experiment 4838, a slight opening of the diaphragm sufficed to interrupt the signal.

Figure 9 additionally shows that the rate of pressure increase within the HPS is more rapid when more powder is used.

Table 2 summarises the important data of the measured shocks. All pressure measurements have been determined from the 20 kHz low pass filtered signal.

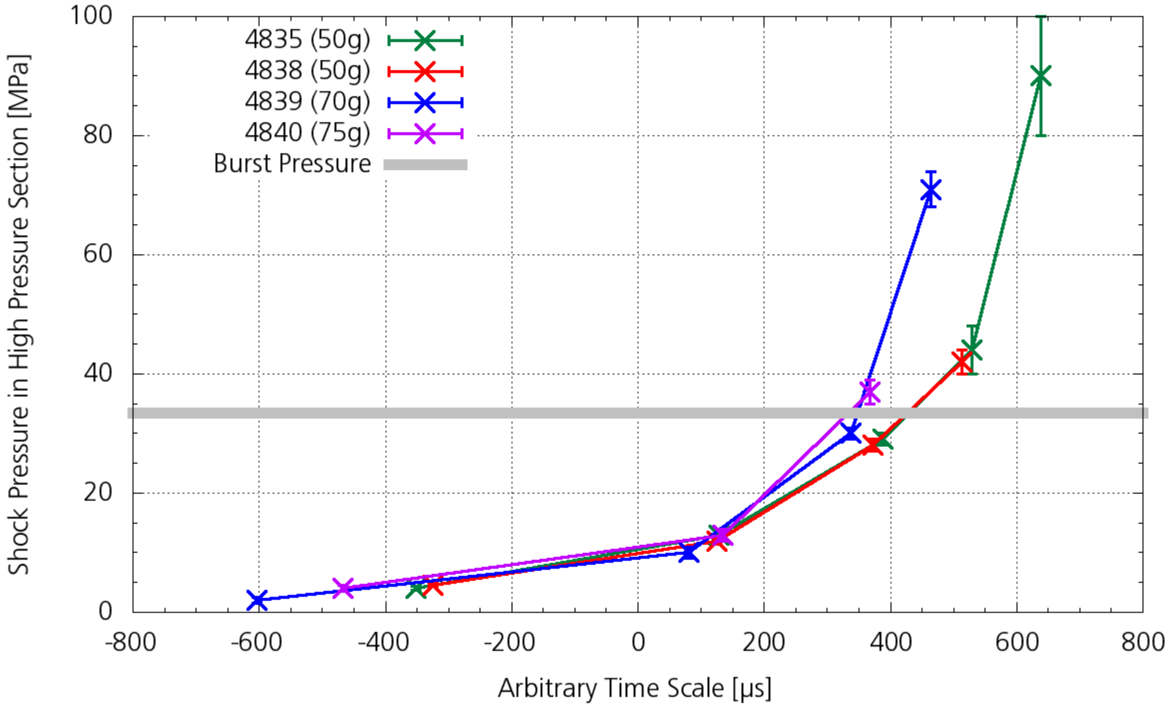

Figure 9: Shock pressure vs. time with the time scale shifted.

Table 2: Shock data.

Experiment	Shock No.	Time of Arrival [µs]	Time Difference to Shock No. 1 [µs]	Pressure in High Pressure Section [MPa]	Remarks
4835	1	–970 ± 10		4.0 ± 0.3	
	2	–490 ± 10	480	13 ± 1	
	3	–230 ± 20	740	29 ± 1	
	4	–90 ± 20	880	44 ± 4	(1)
	5	20 ± 20	990	90 ± 10	(1) (2)
4838	1	–780 ± 10		4.5 ± 0.3	
	2	–330 ± 10	450	12.0 ± 0.5	
	3	–80 ± 20	700	28 ± 1	
	4	58 ± 2	840	42 ± 2	
4839	1	–1 070 ± 1		2.0 ± 0.5	
	2	–386 ± 1	680	10 ± 1	
	3	–129 ± 2	940	30 ± 1	
	4	–2 ± 2	1 070	71 ± 3	
4840	1	–957 ± 1		4.0 ±0.5	
	2	–355 ± 1	600	13 ± 1	
	3	–122 ± 1	840	37 ± 2	

Remarks

(1) In experiment 4835, the oscilloscope settings were not optimised, so that the velocity signal was cut off at ca. ± 3 m/s. This complicates identification of the fourth and fifth shock.

(2) See the above text regarding the fifth shock in experiment 4835.

BURST PRESSURE OF DIAPHRAGM

The measurements show that the acceleration of the piston causes shocks to be generated in the light gas. This is in agreement with theoretical considerations (cf. e. g. [12], section 2.4). The shocks are reflected by the diaphragm, exciting vibrations. A shock with sufficient energy tears the diaphragm open, presumably only partially in the beginning. Further shocks open the diaphragm completely. The opening process of the diaphragm is completed during the initial phase of the acceleration process, before the main compression takes place in the HPS.

Table 3 lists the HPS pressures measured shortly after arrival of the shock prior to, and following burst of the diaphragm. In experiments 4838, 4839 and 4840, the laser beam was adjusted to point to the diaphragm centre. For these experiments it is assumed that the last recorded shock caused the diaphragm to burst, while the second last recorded shock left it intact. In experiment

4835, the velocity was measured closer to the rim of the diaphragm, therefore the fifth shock is ignored in this table and the values are given in brackets only.

It is assumed that the burst pressure is not dependant on the amount of powder used. The values listed in Table 3 support this assumption and indicate a burst pressure between 30 and 37 MPa (300 and 370 bar).

Table 3: HPS Pressure with intact and burst diaphragm.

Experiment	Powder Charge [g]	max. HPS Pressure with Intact Diaphragm [MPa]	HPS Pressure with Burst Diaphragm [MPa]
4835	50	(29)	(44)
4838	50	28	42
4839	70	30	71
4840	75	13	37

PRESSURE SIGNAL NOISE & LIGHT GAS SHOCKS

Attention is drawn to the HPS pressure signal of experiment 4840 near –355 μs, the arrival time of the second shock (Figure 10). The pressure sensor was located 102 mm in front of the diaphragm (see Figure 5). Thus a shock that travelled inside the pump tube first passed the pressure sensor drill hole, then reached the diaphragm where it was reflected, causing the shock to pass the pressure sensor drill hole a second time. The shock excited the light gas inside the drill hole as it passed, which in turn excited the pressure sensor. Both shock arrivals can clearly be identified in the pressure signal. They are marked as "excitation 1" and "excitation 2" in Figure 10, respectively. The shock arrival time at the diaphragm is marked with a vertical line.

It is assumed that the shock excited an acoustic wave in the pressure sensor drill hole (see Figure 5), with a wavelength four times the hole length. Assuming standard* sound speed at this early stage of the acceleration process, the drill hole length of 6 mm corresponds to a wave frequency of 1280 m/s / 4·6 mm = 53 kHz. According to the manufacturer, the eigenfrequency of the sensor† is above 150 kHz. As is shown in Figure 10, the major noise frequency ranges of the signal are 50 to 55 kHz and 150 to 180 kHz, which correspond well to those two values.

Figure 10 allows calculation of the shock speed. The excitation times are –394 μs and –303 μs for the pressure sensor and –355 μs for the diaphragm. The drill hole causes a signal delay of 6 mm / 1.28 mm/μs = 4.7 μs (assuming standard conditions again). The rise time of the pressure sensor† amounts to 2 μs. Thus the shock passes the drill hole at –400.7 μs and –309.7 μs, travelling 45.7 μs from drill hole to diaphragm and 45.3 μs from diaphragm to drill hole. Since the excitation times cannot be determined more precisely than ± 1μs, the two values agree very well. The shock speed equates to 102 mm / 45.5 μs = 2.24 ± 0.05 km/s.

* "Standard" referring to standard conditions: a temperature of 297.15 K and a pressure of 0.1 MPa.

† All sensor properties are taken from the manufacturer's data sheet.

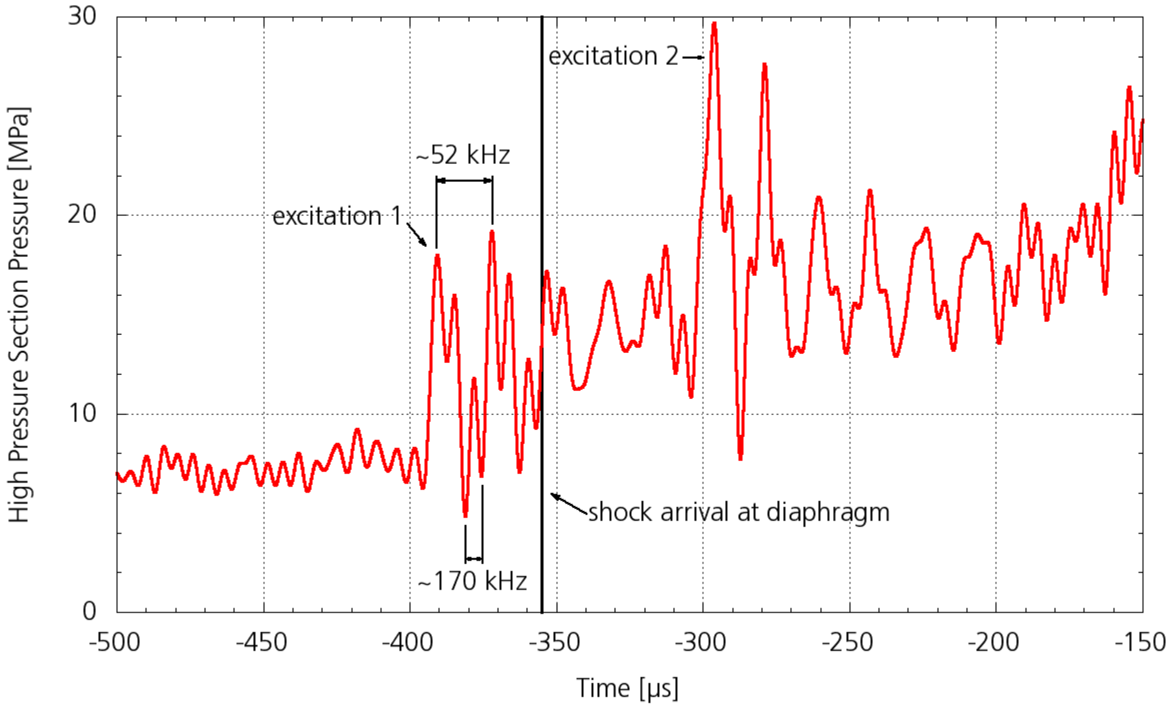

Figure 10: HPS pressure near arrival of second shock.

SUMMARY AND CONCLUSIONS

A convenient method to measure the burst pressure of steel diaphragms used in two-stage light gas guns is presented in which measurements are performed during standard operation of a two-stage light gas gun acceleration cycle with minor modifications, i. e. omitting projectile and sabot. These modifications, being necessary to perform the measurements, have no influence on the gun cycle until the measurements are completed. The obtained burst pressure is therefore regarded as being more realistic than one measured during, for example, quasi-static inflation testing.

Additionally, some interesting insight into the first stage compression cycle is given. The arrival times of the first shocks at the diaphragm location can be measured. Pressure signal noise is analysed and the sources are identified.

REFERENCES

[1] SCHNEIDER, E.; THOMA, K.: *Ausgewählte Kapitel der Kurzzeitdynamik. Teil 5: Hochgeschwindigkeits–impakt*. Freiburg: Fraunhofer Institut für Kurzzeitdynamik, Ernst-Mach-Institut, 1999. - EMI-Bericht 5/99

[2] PUTZAR, R.; SCHÄFER, F.: EMI's new experimental caliber 4 mm light gas gun. In: *Proceedings of the 55th Meeting of the Aeroballistic Range Association*. Freiburg, Germany, 2004

[3] LAMBERT, M.; SCHÄFER, F.; GEYER, T.: Impact damage on sandwich panels and multi-layer insulation. In: *International Journal of Impact Engineering* 26 (2001), No. 1, pp. 369-380

[4] PUTZAR, R.; SCHÄFER, F.; ROMBERG, O.; LAMBERT, M.: Vulnerability of shielded fuel pipes and heat pipes to hypervelocity impacts. In: *Proceedings of the 4th European Conference on Space Debris*. ESOC, Darmstadt, Germany, 2005. - ESA SP-587, pp. 459-464

[5] PUTZAR, R.; SCHÄFER, F.; STOKES, H.; CHANT, R.; LAMBERT, M.: Vulnerability of spacecraft electronics boxes to hypervelocity impacts. In: *Proceedings of the 56th International Astronautical Congress 2005*. Fukuoka, Japan, 2005. - IAC-05-B6.4.02

[6] SCHÄFER, F.: The threat of space debris and micrometeoroids to spacecraft operations. In: *ERCIM News* 65 (2006), pp. 27-29

[7] SCHÄFER, F.; DESTEFANIS, R.; RYAN, S.; RIEDEL, W.; LAMBERT, M.: Hypervelocity impact testing of CFRP/Al honeycomb satellite structures. In: *Proceedings of the 4th European Conference on Space Debris*. ESOC, Darmstadt, Deutschland, 2005. - ESA SP-587, S. 407-412

[8] SCHÄFER, F.; GEYER, T.; SCHNEIDER, E.; ROTT, M.; IGENBERGS, E.: Degradation and destruction of optical surfaces by hypervelocity impact. In: *International Journal of Impact Engineering* 26 (2000), pp. 683-698

[9] SCHNEIDER, E. E.; SCHÄFER, F. K.: Hypervelocity impact research: Acceleration technology and applications. In: *Advances in Space Research* 28 (2001), No. 9, pp. 1417-1424

[10] SCHNEIDER, E. E.; SCHÄFER, F. K.; DESTEFANIS, R.; LAMBERT, M.: Advanced shields for manned space modules. In: *Proceedings of the 55th International Astronautical Congress 2004*. Vancouver, Canada, 2004

[11] THOMA, K.; RIEDEL, W.; SCHÄFER, F. K.; HIERMAIER, S.: Status and perspectives in protective design. In: *Space Debris* 2 (2000), No. 4, pp. 201-224

[12] CANNING, T. N.; SEIFF, A.; JAMES, C. S.: *Ballistic-range technology*. Neuilly sur Seine, Frankreich: North Atlantic Treaty Organization (NATO), Advisory Group for Aerospace Research and Development (AGARD), 1970. - AGARDograph No. 138